PHYSICAL SCIENCES

Low-energy transmission electron diffraction and imaging of large-area graphene

Wei Zhao,[1]* Bingyu Xia,[1]* Li Lin,[2]* Xiaoyang Xiao,[1]* Peng Liu,[1†] Xiaoyang Lin,[1,3] Hailin Peng,[2] Yuanmin Zhu,[4] Rong Yu,[4] Peng Lei,[1] Jiangtao Wang,[1] Lina Zhang,[1] Yong Xu,[1,5,6] Mingwen Zhao,[7] Lianmao Peng,[8] Qunqing Li,[1,6] Wenhui Duan,[1,6] Zhongfan Liu,[2] Shoushan Fan,[1,6] Kaili Jiang[1,6†]

Two-dimensional (2D) materials have attracted interest because of their excellent properties and potential applications. A key step in realizing industrial applications is to synthesize wafer-scale single-crystal samples. Until now, single-crystal samples, such as graphene domains up to the centimeter scale, have been synthesized. However, a new challenge is to efficiently characterize large-area samples. Currently, the crystalline characterization of these samples still relies on selected-area electron diffraction (SAED) or low-energy electron diffraction (LEED), which is more suitable for characterizing very small local regions. This paper presents a highly efficient characterization technique that adopts a low-energy electrostatically focused electron gun and a super-aligned carbon nanotube (SACNT) film sample support. It allows rapid crystalline characterization of large-area graphene through a single photograph of a transmission-diffracted image at a large beam size. Additionally, the low-energy electron beam enables the observation of a unique diffraction pattern of adsorbates on the suspended graphene at room temperature. This work presents a simple and convenient method for characterizing the macroscopic structures of 2D materials, and the instrument we constructed allows the study of the weak interaction with 2D materials.

INTRODUCTION

Since graphene was discovered in 2004, two-dimensional (2D) materials have attracted interest because of their unique properties and potential applications (*1*–*4*). A major challenge in this field is how to synthesize wafer-scale single-crystal 2D materials. Some progress has been made in this direction; for example, millimeter- to centimeter-scale single-crystal graphene domains have been successfully synthesized (*5*–*12*). However, the characterization of the crystalline quality of large-area graphene still relies on selected-area electron diffraction (SAED) in transmission electron microscopy (TEM) or low-energy electron diffraction (LEED). For SAED, the limited aperture size and TEM grid size make it time-consuming to completely map the crystal orientation distribution of large-area samples (see note S1). For LEED, the adsorbates on a surface could affect the LEED signal. Hence, an ultrahigh vacuum system and a long-time annealing process are imperative to obtain a sharp LEED pattern. However, LEED systems are vulnerable to interference from substrates. In general, we have no option but to select some representative regions of large-area 2D materials and assume that these regions can represent the global structural information of the whole sample. An effective method and instrument for characterizing the crystalline nature of large-area 2D materials are still lacking.

We present a method and an apparatus for the rapid crystalline characterization of centimeter-scale graphene via large-scale low-energy transmission electron diffraction and imaging. This enables us to rapidly acquire the structural information of a large-area sample through a single photograph of a diffracted image. An electrostatically focused electron gun is used as an electron source, generating an electron beam of sizes varying from 400 μm to 1 cm in diameter. Because the electron beam is large enough, no lenses are used to magnify the electron image after electrons pass through the graphene. Therefore, no aberration is introduced in the images or diffraction patterns. Low-energy electrons (200 eV to several keV) are used to avoid damaging the one-atom-thick graphene. As a consequence, the diffraction contrast of graphene is higher than that in TEM. Another key technique is the use of a low-noise super-aligned carbon nanotube (SACNT) film as sample support, which has negligible influence on the diffraction pattern and image acquisition (see note S2). An SACNT film of centimeter scale can be freestanding, thus supporting large-area 2D materials. In summary, the two techniques, a large-scale low-energy electron beam and a large-area SACNT film as sample support, enable the rapid and convenient characterization of large-area graphene and the study of the adsorbates on it. Previous studies of the adsorption on graphene frequently used LEED to acquire the diffraction pattern of the adsorption structure (*13*, *14*), which could not eliminate the interference of the substrate underneath the graphene (*15*–*17*). The presented techniques allow the study of the intrinsic interaction of the adsorbates and the graphene. A unique diffraction pattern of adsorbates, presumed to be water molecules, on graphene at room temperature was observed. Invoked by the chain model of polymer adsorption on graphene (*18*), we proposed a presumed chain-based submonolayer structure to explain the diffraction pattern of the adsorbates. Large-area polycrystalline chemical vapor deposition (CVD) MoS_2 samples were also studied using the new method. This new method and the instrument we constructed will promote future research on 2D materials.

[1]State Key Laboratory of Low-Dimensional Quantum Physics, Department of Physics and Tsinghua-Foxconn Nanotechnology Research Center, Tsinghua University, Beijing 100084, China. [2]Center for Nanochemistry, Beijing Science and Engineering Center for Nanocarbons, Beijing National Laboratory for Molecular Sciences, College of Chemistry and Molecular Engineering, Peking University, Beijing 100871, China. [3]Fert Beijing Research Institute, School of Electrical and Information Engineering, Big Data and Brain Computing (BDBC), Beihang University, Beijing 100191, China. [4]National Center for Electron Microscopy in Beijing, School of Materials Science and Engineering, Tsinghua University, Beijing 100084, China. [5]RIKEN Center for Emergent Matter Science, Wako, Saitama 351-0198, Japan. [6]Collaborative Innovation Center of Quantum Matter, Beijing 100084, China. [7]School of Physics and State Key Laboratory of Crystal Materials, Shandong University, Jinan, Shandong 250100, China. [8]Key Laboratory for the Physics and Chemistry of Nanodevices, Department of Electronics, Peking University, Beijing 100871, China.
*These authors contributed equally to this work.
†Corresponding author. Email: pengliu@tsinghua.edu.cn (P.L.); JiangKL@tsinghua.edu.cn (K.J.)

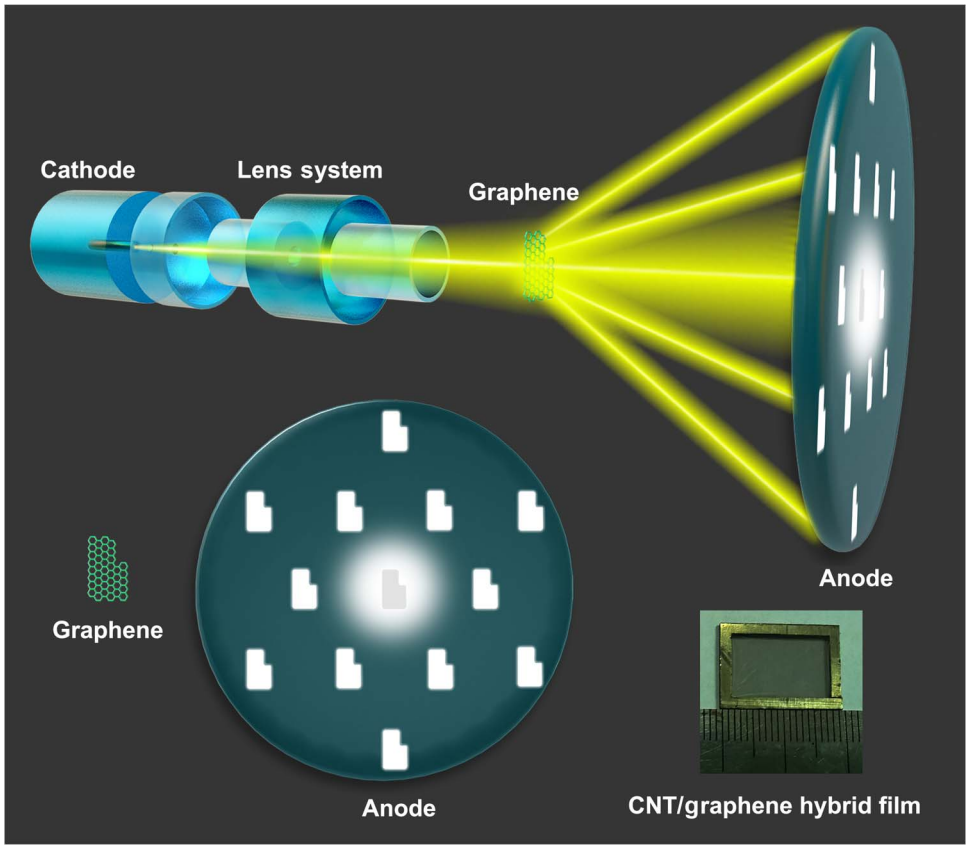

Fig. 1. Schematic of the low-energy transmission electron diffraction system. Thermionic cathode, lens system, graphene sample, SACNT film sample support (not shown), and phosphor anode. The lens system can be tuned to generate electron beams of variable size (from 400 μm to 1 cm in diameter). The front view of the graphene sample and anode is shown. The inset at the bottom right shows a photograph of a CNT/graphene hybrid film (CGF) more than 1.6 cm long.

RESULTS

Experimental scheme and setup

The diffraction system is a very simple implementation of electron microscopy, no more complicated than a point-projection microscope (*19*, *20*). It comprises of only an electron source, a nearby sample, and an electron imaging screen some distance away. Figure 1 presents the simplified configuration of the diffraction system. An electrostatically focused electron gun composed of a thermionic cathode and lens system is used as the electron source. Graphene is suspended on two layers of cross-stacking SACNT films, forming a CNT/graphene hybrid film (CGF) (*21*). The SACNT film with the network structure exhibited excellent mechanical performance, allowing it to suspend graphene of centimeter scale (inset of Fig. 1, showing a CGF sample more than 1.6 cm long). A metal frame is used as the CGF sample holder (not plotted in Fig. 1). A phosphor anode, placed behind the CGF sample, is used as the imaging screen. All of these parts work in a vacuum of approximately 10^{-3} to 10^{-5} Pa. By adjusting the lens system, electrons generated from the cathode can be focused (400 μm to 1 cm in diameter) and accelerated (200 eV to several keV) through the CGF. Some electrons are diffracted at specific angles depending on the in-plane lattice spacings of the graphene, forming diffraction patterns. For a single-crystal graphene domain, when the electron beam is tuned to be large enough to cover the whole sample, there is only one set of hexagonal diffraction patterns of the same shape as the graphene domain on the anode, as shown in Fig. 1. Thus, the single-crystalline nature of a graphene domain can be revealed through a single photograph of a diffracted image. When the electron beam is focused to 400 μm, the diffraction pattern, like an SAED pattern, can also be acquired (see note S3). The angle θ between the incident electron beam and the diffracted electron beam satisfies the equation

$$d \sin\theta = \lambda \quad (1)$$

Here, λ represents the wavelength of the electrons, and d represents the in-plane lattice spacing of graphene. The diffraction formula is slightly different from the conventional Bragg equation. A detailed explanation is presented in note S3.

Characterization of large-area single-crystal graphene

A large-area single-crystal graphene synthesis approach was used by combining a multistage carbon supply and second passivation (*22*). Figure 2 (A and B) shows photographs of graphene islands on a copper foil, which was oxidized in air at 200°C to make the graphene islands optically visible (*23*). Two islands, denoted as 1 and 2 in Fig. 2B, were investigated in detail. These graphene islands were transferred onto the SACNT film, forming a centimeter-scale CGF sample (*21*). Figure 2C shows the photograph of the CGF sample, including graphene islands 1 and 2. The sample was then placed in the electron diffraction system. When the electron beam was enlarged to cover the entire graphene island 1, the diffracted image of this graphene island could be observed, as shown in Fig. 2 (D and E). It is similar in appearance to the shadow image in convergent beam electron diffraction (*24*–*26*) or the multiple

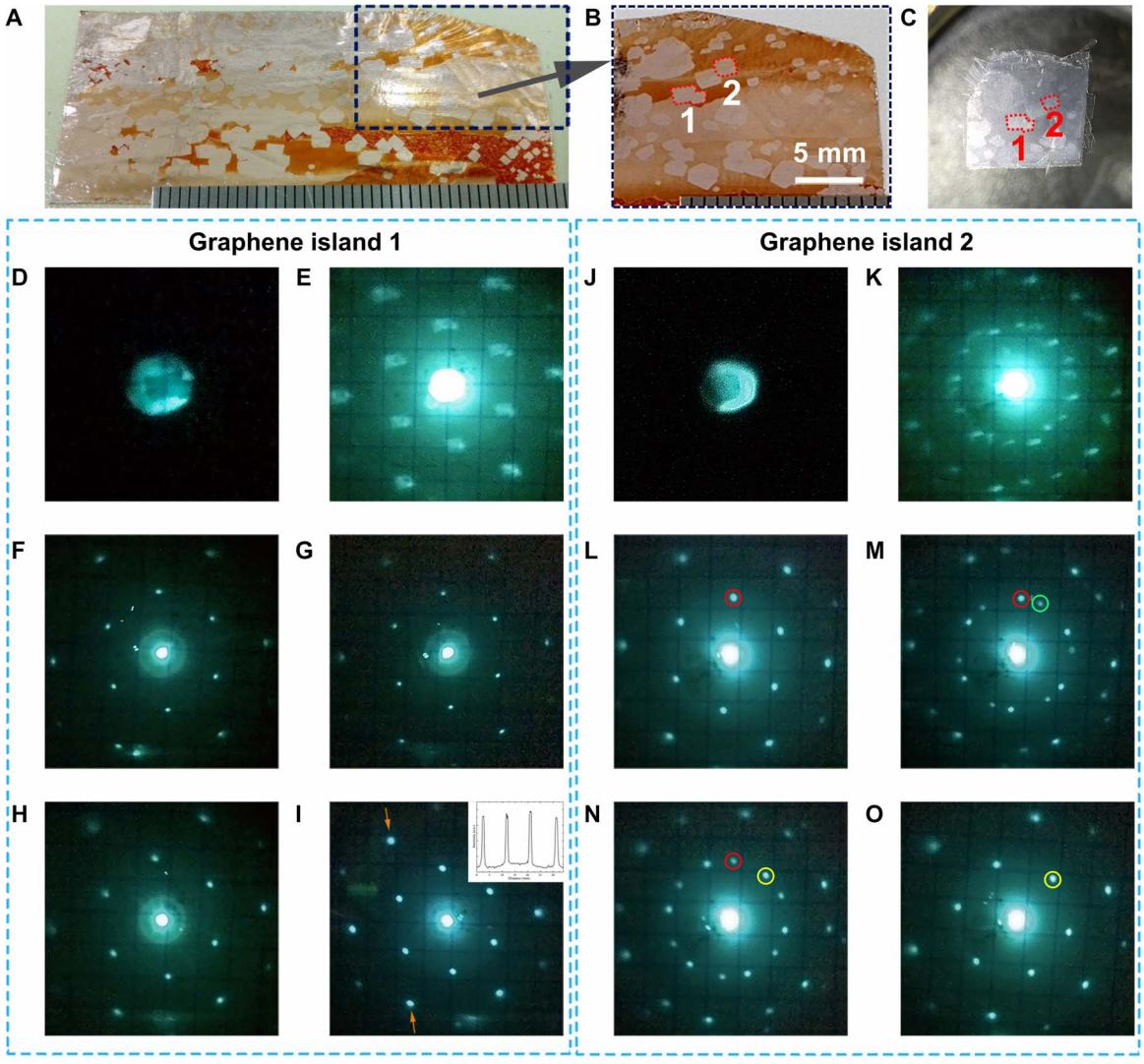

Fig. 2. Transmission electron diffraction and imaging of large-area graphene islands. (**A** and **B**) Photographs of large-area CVD graphene islands grown on copper. The graphene islands surrounded by red dashed lines are denoted as graphene islands 1 and 2. (**C**) Photograph of CGF prepared from copper/graphene in (B). Graphene islands 1 and 2 are denoted by red dashed lines. (**D**) Image of graphene island 1 in central spot. The exposure time is 0.01 s. (**E**) Diffracted image of graphene island 1 in diffraction spots. The exposure time is 1 s. (**F** to **I**) Diffraction patterns corresponding to different regions of graphene island 1. Inset shows profile plot of diffraction spot peak intensities along arrows in (I). (**J**) Image of graphene island 2 in central spot. The exposure time is 0.01 s. (**K**) Diffracted image of graphene island 2 in diffraction spots. The exposure time is 0.5 s. (**L** to **O**) Diffraction patterns corresponding to different regions of graphene island 2. Each set of

dark-field image (*27*). Shadow imaging and multiple dark-field imaging can only be used to characterize very small local regions of nanometer to micrometer scale. For larger regions, the diffraction disks overlap because of the small diffraction angle in TEM. In contrast, the angle corresponding to {10-10} diffraction spots of graphene in the diffraction system can be as large as 9°. As shown, each part of the diffracted image in Fig. 2E is separated, comprising of a hexagonal diffraction pattern, and the shape of the diffracted image is the same as that of graphene island 1. Thus, the single-crystalline nature of graphene island 1 is directly identified from a single photograph. For graphene island 2, when the electron beam covered the entire sample, the image of this graphene island in the central spot could be observed, as shown in Fig. 2J (similar to that in Fig. 2D), but the diffracted image became very complex, as shown in Fig. 2K. Because the electrons passing through different graphene domains will be diffracted at different azimuthal angles, the diffracted image is a superposition corresponding to each graphene domain (Fig. 2K). Thus, we can rapidly distinguish whether a graphene island is a single crystal on the basis of its diffracted image, which simultaneously shows the diffraction pattern and image of a large-area sample.

When the electron beam in the diffraction system was focused to a small size, a diffraction pattern, similar to the SAED pattern, could be achieved for both graphene island 1 (Fig. 2, F to I) and graphene island 2 (Fig. 2, L to O). The diffraction patterns of graphene island 1 at different positions show the same set of hexagonal diffraction spots without rotation, again confirming that graphene island 1 is a single crystal. In contrast, the diffraction patterns of graphene island 2 at different positions show three sets of hexagonal diffraction spots, indicating that graphene island 2 is composed of at least three single-crystal graphene

domains. Thus, a detailed analysis of the crystalline nature can also be realized via a fast scan of electron diffraction patterns (see movies S1 and S2). Whether by using the diffracted image or via a fast scan, the characterization of large-area graphene is more efficient than the commonly used SAED. As a rough estimation based on beam size and aperture size, SAED will require time approximately 8 orders of magnitude greater than that of the presented method required to completely characterize the crystalline nature of a graphene island of centimeter scale (see note S1). To demonstrate the power of our technique, we performed a 2D spatial mapping of a submillimeter graphene island (see note S4).

Characterization of the crystal orientation distribution of large-area polycrystalline graphene

For a large-area polycrystalline graphene composed of graphene domains much smaller than the electron beam size, the method can be used to acquire the crystal orientation distribution of the sample. Figure 3A shows the optical image of the large-area continuous polycrystalline graphene transferred onto a silicon substrate (with a 300-nm SiO_2 layer). The homogeneous optical contrast indicates that the sample is a uniform monolayer graphene. The SAED pattern shown in Fig. 3B also confirms that the graphene is monolayer (see note S5). The diffracted image of polycrystalline graphene taken in the diffraction system is shown in Fig. 3C. Different from Fig. 2E and Fig. 3B, two sets of hexagonal diffraction patterns appear in Fig. 3C. When the electron beam diameter was decreased (to approximately 400 μm; see note S6), the diffraction pattern also revealed two sets of hexagonal diffraction spots, as shown in Fig. 3D. Because the graphene sample was verified to be monolayer via optical (Fig. 3A) and TEM characterization (see note S5), the results shown in Fig. 3 (C and D) reveal the crystal orientation distribution of the large-area polycrystalline graphene. Because the graphene is polycrystalline composed of small single-crystal graphene domains of micrometer scale, the diffraction pattern is a superposition of diffraction patterns of many small-sized graphene domains. The two sets of diffraction patterns indicate that the polycrystalline graphene at millimeter scale has two preferred crystal orientations. With the large-scale electron beam, the global crystal orientation distribution of large-area polycrystalline graphene can be ascertained.

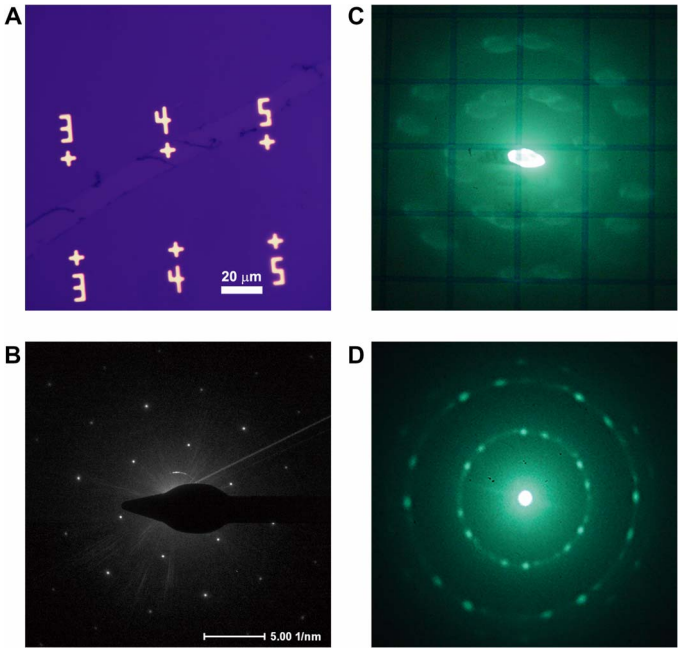

Fig. 3. Transmission electron diffraction and imaging of large-area continuous polycrystalline graphene. (**A**) Optical image of transferred large-area continuous polycrystalline graphene on silicon substrate (with SiO_2 layer). (**B**) SAED pattern of polycrystalline graphene (200 keV), with an aperture size of 100 nm. (**C**) Transmission electron diffracted image of large-area continuous polycrystalline graphene.

Investigations of the relation between the copper substrate and the crystal orientation of graphene have used LEED to determine the crystal orientation distribution of large-area graphene (*28*, *29*). The diffraction system presented is also able to do that. In addition, the diffraction pattern obtained does not contain interference from the copper substrate. On each single-crystal copper grain approximating (100) face, there are two preferred crystal orientations for graphene growth, although the exact orientation angle may vary depending on the Miller indices of the copper grain (see note S7). The crystal orientation distribution of large-area MoS_2 can also be studied using the presented method, although there seems to be no preferred crystal orientation for MoS_2 growth on SiO_2 (see note S8).

Diffraction of adsorbates on graphene

The relatively low-energy electron beam required (as low as 200 eV) in the diffraction system is suitable for the investigation of adsorption, which has been intensely studied for years (*13*, *14*, *30*–*33*). With the rise of 2D materials, the adsorption on graphene has become a new research direction in recent years (*13*, *14*, *34*, *35*). In this diffraction system, we have studied the adsorption on graphene at room temperature. For the newly prepared CGF, a set of hexagonal diffraction spots appeared near the central spot, as shown in Fig. 4A. These extra diffraction spots gradually disappeared after a few seconds of electron irradiation (Fig. 4, B to D). When the electron energy was kept as low as 200 eV and the electron beam current was decreased, these extra diffraction spots remained stable for hours (see note S9). When the electron beam was moved to a new position, the extra diffraction pattern was observed and then disappeared again (see movies S3 and S4). As has been found in LEED, the adsorption on graphene will cause an extra diffraction pattern, and electron irradiation can induce desorption (*13*). The extra diffraction pattern in this experiment is likely the result of adsorption. Because adsorption/desorption is a metastable phenomenon and sensitive to temperature, we heated the CGF to incandescence in vacuum and found that no extra diffraction spots could be observed in the diffraction pattern. A similar extra diffraction pattern was observed via LEED in a polymer/graphene bilayer system and was attributed to the diffraction of the polymer (*18*). However, in this experiment, the extra diffraction pattern could not be the result of the polymer because no polymer was introduced in the graphene transfer process and electron diffraction operation. Because the CGF was rinsed in deionized (DI) water during preparation and no other chemical agents were subsequently introduced, water is one of the possible adsorbate species. Regarding the CGF sample without an extra diffraction pattern after electron irradiation or after being heated (Fig. 4, I and J), water mist was sprayed onto it for approximately 2 min (Fig. 4M). The extra diffraction pattern was found to appear again (Fig. 4N). Similar to before, this diffraction pattern disappeared again because of electron irradiation (see movie S5). In addition to single-crystal graphene, the diffraction pattern of the adsorbates can also be seen for polycrystalline graphene. Figure 4 (G and K) shows the diffraction patterns of the adsorbates on polycrystalline graphene with two and three crystal orientations,

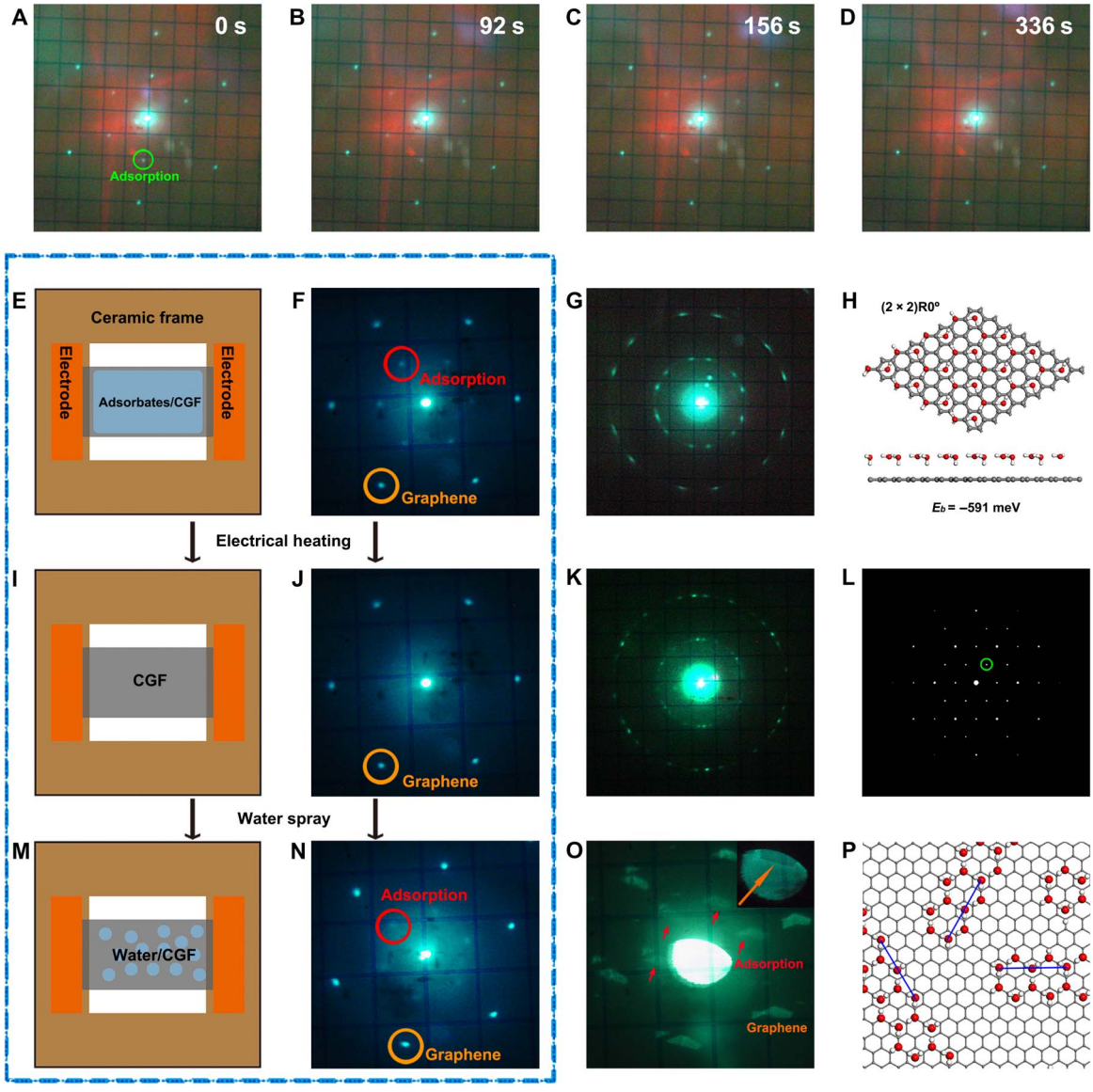

Fig. 4. Transmission electron diffraction pattern of adsorbates (presumed to be water molecules) on both single-crystal graphene and polycrystalline graphene. (**A** to **D**) Observation and gradual disappearance of transmission electron diffraction patterns of adsorbates on single-crystal graphene. One of the diffraction spots of adsorption is marked with a green circle in (A). The exposure time was fixed at 15 s for each image. The red background of the phosphor anode was caused by the incandescence of the thermionic cathode. (**E**) Schematic of the CGF (after rinsing with DI water) supported on a ceramic frame with electrodes. (**F**) A typical diffraction pattern of adsorbates on graphene corresponding to (E). (**I**) Schematic of the CGF after electrical heating. The adsorbates are completely desorbed from the graphene. (**J**) A typical diffraction pattern of graphene without adsorbates corresponding to (I). (**M**) Schematic of the CGF after water spray treatment. (**N**) A typical diffraction pattern of water adsorption on graphene corresponding to (M). The diffraction spots corresponding to adsorbates and graphene are indicated in (F), (J), and (N). (**G** and **K**) Transmission electron diffraction patterns of adsorbates on graphene with two and three main crystal orientations, respectively. (**O**) Diffracted image of adsorbates on graphene. The diffracted images of adsorbates and graphene are marked with arrows. Inset at the top right shows the image of the graphene island in the central spot. (**H**) Calculated adsorption structure for monolayer (2 × 2)R0° water adsorption on graphene. Gray, red, and white spheres represent carbon, oxygen, and hydrogen atoms, respectively. The binding energy per molecule E_b is shown. (**L**) Simulation of diffraction pattern for monolayer (2 × 2)R0° water adsorption on graphene. The (10-10) diffraction spot of water adsorption is marked with a green circle. (**P**) Schematic of the ice-chain model for water adsorption on graphene. Gray, red, and white spheres represent carbon, oxygen, and hydrogen atoms, respectively. The three equivalent orientations of the ice chains are indicated.

respectively. In each of them, the orientations of the diffraction spots caused by the adsorbates match the crystal orientations of the graphene, and the in-plane lattice spacing corresponding to these diffraction spots is twice the length of the {10-10} lattice spacing of the graphene. Beyond the diffraction spots of the adsorbates, the diffracted image of the adsorbates was also obtained when the electron beam was enlarged, as shown in Fig. 4O. It shows the same shape and orientation of the diffracted image of the graphene in the diffraction spots, indicating that the adsorbates are highly correlated with the graphene lattice at a large scale.

On the basis of the existing experimental results, we presumed the adsorbates on graphene to be water molecules. Water adsorption on

graphene has been theoretically and experimentally investigated by many groups (*13*, *14*, *35*–*40*). The experiments were all carried out with graphene on a substrate such as platinum, silicon, and iridium (*13*, *14*, *35*, *37*, *38*, *40*). However, the substrate underneath the graphene may influence the adsorption itself. Li *et al.* (*16*) found that water adsorption on graphene can be enhanced (adsorption energy increased by up to 30%) in the presence of underlying metal substrates. For epitaxial graphene on a Ru(0001) substrate, it has been reported that water adsorbates will efficiently split the graphene (*17*). Because the graphene in the diffraction system is suspended on an SACNT network, the influence of the substrate can be reduced, which is a big advantage of the diffraction system.

We presumed the adsorbates on the graphene to be water molecules and performed first-principles calculations to characterize the possible adsorption configurations (see method details in note S10). The key physical quantity needed to discuss structural stability is the binding energy per molecule E_b defined as the energy difference between the adsorption system and the isolated graphene and molecules divided by the number of molecules. The primary contributor to E_b is the hydrogen bonds between H_2O molecules, and the secondary contributor is the van der Waals coupling between H_2O and graphene. The adsorption structure was not the $(\sqrt{3} \times \sqrt{3})$R30° ice structure that has been theoretically studied (*15*, *16*) because it is inconsistent with those experimental results. We found that (2×2)R0° is a stable structure with an E_b of −591 meV (see Fig. 4H). The simulated {10-10} diffraction spots of monolayer (2×2)R0° structure (see Fig. 4L) were consistent with the diffraction pattern of the water adsorption we observed, as shown in Fig. 4A. However, no other diffraction spots corresponding to higher Bravais-Miller indices of (2×2)R0° water adsorption were observed in Fig. 4A.

The LEED characterization of the polymer/graphene bilayer system also revealed only six extra diffraction spots, which is almost the same result as that of the presented diffraction system and was attributed to the folded-chain structure of poly(methyl methacrylate) (*18*). Studies have shown that water also tends to form a chain structure on some substrates (*41*, *42*). Inspired by these reports, we presumed that the adsorbates on graphene may be submonolayer ice chains of quasi–long-range order. These ice chains show three equivalent crystal orientations of the same binding energy (Fig. 4P). Because the electron beam size in the diffraction system is large enough, the observed diffraction pattern of water adsorption is a superposition of diffraction patterns of these ice chains of three orientations. If the electron beam is small and only covers ice chains of single-crystal orientation, there will be only one pair of diffraction spots of water adsorption. The diffraction results of the cryogenic TEM (cryo-TEM) characterization might support this presumption (see note S11 and movies S6 and S7). The observation of the unique adsorbates on the graphene through transmission electron diffraction in the experiment creates opportunities for further research in related areas. Although there is no conclusive experimental evidence to confirm the adsorbate species on graphene, we have demonstrated the power of the diffraction system in studying weak interaction phenomena with graphene.

Construction of a compact instrument

Considering the wide spectrum of potential applications in 2D materials, we designed and constructed a compact instrument, as shown in Fig. 5A. This instrument can do the same job as the diffraction system. Figure 5B shows the transmission electron diffraction pattern taken by this instrument. With the help of a microchannel plate (MCP), the diffraction spots of graphene and the adsorbates on it can be seen at normal illumination. Benefiting from miniaturization, this diffraction instrument can be applied in various occasions. A field emission gun (FEG) can also be used as an electron source to produce the diffraction pattern of the graphene (see note S12).

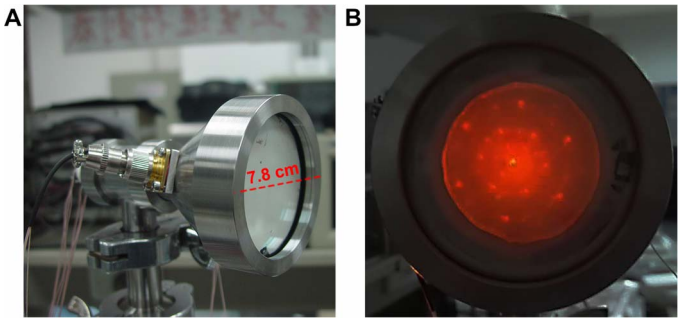

Fig. 5. A compact instrument for transmission electron diffraction and imaging. (**A**) Photograph of the compact instrument. (**B**) Transmission electron diffraction pattern of polycrystalline graphene acquired by using the compact instrument. With the help of an MCP, the diffraction spots of adsorbates and graphene can be seen at normal illumination.

DISCUSSION

We have realized the rapid crystalline characterization of centimeter-scale graphene via low-energy transmission electron diffraction and imaging. Large-area single-crystal graphene domains of millimeter scale can be easily verified through a single photograph of a diffracted image. The crystal orientation distribution of large-area polycrystalline graphene can be acquired via a fast scan. Additionally, a unique diffraction pattern of the adsorbates on the suspended graphene at room temperature can be observed. Because of the excellent mechanical performance and high electron transparency, the SACNT film, as a large-area sample support, yields advantages in electron diffraction and imaging. Large-area MoS_2 can also be characterized by using this method (see note S8). The presented method can be helpful for studying weak interaction phenomena with 2D materials and in situ synthesis on 2D materials at a wide range of temperatures. The presented compact instrument is expected to be useful in applications in both the academic research and industrial production of 2D materials.

MATERIALS AND METHODS

Synthesis of large-area single-crystal graphene domains

The first step is nucleation control. Commercially available copper foils (25 μm thick; 99.8%, Alfa Aesar) were electrochemically polished using a polishing solution to clean the surface. Graphene was synthesized on a copper foil in a low-pressure CVD (LPCVD) system equipped with a quartz tube 2.54 cm in diameter. To grow graphene, the system was heated to 1020°C under H_2 flow of 100 standard cubic centimeter per minute (sccm) at 110 Pa. The annealing was carried out for 1 hour at 1020°C to eliminate surface oxygen and contamination. After the annealing process, the first passivation for nucleation control was initiated by heating the copper for 30 min at 1020°C without gas at a pressure of 1 Pa. Subsequently, CH_4 and H_2 were introduced into the LPCVD system for the graphene growth at 1020°C under different H_2/CH_4 ratios. The growth time was set to 5 min to form a small nucleus for subsequent rapid growth. The next step is second passivation

and speed-up. After the nucleation-control step, the second passivation effect was carried out on the copper surface by shutting down the H_2 and CH_4 and heating without reducing the gas. During this step, the pressure of the system was nearly 1 Pa. In addition, the remaining gas, consisting of O_2, resulted in the second passivation. The treatment time was set to 1 to 3 min to etch the original nuclei. The rapid growth of large single-crystal graphene was initiated by introducing CH_4 and H_2. Finally, the sample was moved from the high-temperature zone to a room-temperature zone with the same gas flow using a magnet. Details of this method can be found in the study of Lin *et al.* (*22*).

Synthesis of large-area continuous polycrystalline graphene

The CVD method was used to grow large-area continuous polycrystalline graphene. Copper foils (25 μm thick; 99.8%, Alfa Aesar) were loaded into an LPCVD system equipped with a quartz tube 2.54 cm in diameter. The LPCVD system was heated to 1040°C for 40 min with H_2 (5 sccm) followed by annealing for 30 min. The system pressure was kept at 13 Pa. Then, CH_4 (30 sccm) was introduced as the carbon source for graphene growth for 20 min at a pressure of 66 Pa. Finally, the system was cooled down naturally with H_2 (5 sccm) and CH_4 (30 sccm).

Preparation of CGF

Because graphene was grown on both sides of the copper foil, an oxygen reactive-ion etching process was used to remove graphene from one side (bottom) of the foil. Then, two layers of SACNT films were cross-stacked on top of the graphene. The copper foil was etched by using an ammonium persulfate solution (0.1 M), resulting in a free-standing CGF sample floating on the surface of the solution. The CGF sample was thoroughly washed with DI water and then transferred to the diffraction system.

SUPPLEMENTARY MATERIALS

Supplementary material for this article is available at http://advances.sciencemag.org/cgi/content/full/3/9/e1603231/DC1

note S1. SAED with different aperture sizes.
note S2. Transmission electron diffraction of SACNT films.
note S3. Transmission electron diffraction of graphene.
note S4. 2D spatial mapping of a graphene island.
note S5. Monolayer characterization of graphene using SAED and the diffraction system.
note S6. Estimation of transmission electron beam size.
note S7. Transmission electron diffraction mapping of polycrystalline graphene.
note S8. Crystalline characterization of large-area polycrystalline MoS_2.
note S9. Diffraction pattern of adsorbates on suspended graphene.
note S10. Calculation of adsorption structure of water on graphene.
note S11. Cryo-TEM characterization of adsorbates on graphene.
note S12. CNT field emitter as cathode.
fig. S1. SAED patterns of polycrystalline graphene with different apertures.
fig. S2. Transmission electron diffraction pattern of SACNT films.
fig. S3. Transmission electron diffraction of graphene.
fig. S4. 2D spatial mapping of a graphene island.
fig. S5. Monolayer characterization of graphene using SAED and the diffraction system.
fig. S6. Estimation of transmission electron beam size.
fig. S7. Transmission electron diffraction of large-area polycrystalline graphene.
fig. S8. Transmission electron diffraction mapping of polycrystalline graphene.
fig. S9. Transmission electron diffraction of MoS_2.
fig. S10. Diffraction pattern of adsorbates on polycrystalline graphene.
fig. S11. Adsorption of a single H_2O molecule on a 4 × 4 supercell of graphene.
fig. S12. A ($\sqrt{3} \times \sqrt{3}$)R30° superstructure of water adsorbed on graphene.
fig. S13. A hexagonal ring of water adsorbed on an 8 × 8 supercell of graphene.
fig. S14. Diffraction spots of adsorbates on graphene in cryo-TEM.
fig. S15. Transmission electron diffraction pattern of graphene acquired using a CNT FEG.
table S1. Data for calculation of the transmission electron beam size.
movie S1. Crystalline characterization of a single-crystal graphene island.
movie S2. Crystalline characterization of a polycrystalline graphene island.
movie S3. Diffraction pattern of adsorbates on graphene.
movie S4. Another diffraction pattern of adsorbates on graphene.
movie S5. Diffraction pattern of water adsorption on graphene after water spray.
movie S6. Diffraction pattern of adsorbates of one crystal orientation on graphene in cryo-TEM.
movie S7. Diffraction pattern of adsorbates of two crystal orientations on graphene in cryo-TEM.
References (*43*–*52*)

REFERENCES AND NOTES

1. K. S. Novoselov, A. K. Geim, S. V. Morozov, D. Jiang, Y. Zhang, S. V. Dubonos, I. V. Grigorieva, A. A. Firsov, Electric field effect in atomically thin carbon films. *Science* **306**, 666–669 (2004).
2. A. K. Geim, Graphene: Status and prospects. *Science* **324**, 1530–1534 (2009).
3. Q. H. Wang, K. Kalantar-Zadeh, A. Kis, J. N. Coleman, M. S. Strano, Electronics and optoelectronics of two-dimensional transition metal dichalcogenides. *Nat. Nanotechnol.* **7**, 699–712 (2012).
4. L. Li, Y. Yu, G. J. Ye, Q. Ge, X. Ou, H. Wu, D. Feng, X. H. Chen, Y. Zhang, Black phosphorus field-effect transistors. *Nat. Nanotechnol.* **9**, 372–377 (2014).
5. L. B. Gao, W. Ren, H. Xu, L. Jin, Z. Wang, T. Ma, L.-P. Ma, Z. Zhang, Q. Fu, L.-M. Peng, X. Bao, H.-M. Cheng, Repeated growth and bubbling transfer of graphene with millimetre-size single-crystal grains using platinum. *Nat. Commun.* **3**, 699 (2012).
6. Z. Yan, J. Lin, Z. Peng, Z. Sun, Y. Zhu, L. Li, C. Xiang, E. L. Samuel, C. Kittrell, J. M. Tour, Toward the synthesis of wafer-scale single-crystal graphene on copper foils. *ACS Nano* **6**, 9110–9117 (2012).
7. L. Gan, Z. Luo, Turning off hydrogen to realize seeded growth of subcentimeter single-crystal graphene grains on copper. *ACS Nano* **7**, 9480–9488 (2013).
8. T. Wu, G. Ding, H. Shen, H. Wang, L. Sun, D. Jiang, X. Xie, M. Jiang, Triggering the continuous growth of graphene toward millimeter-sized grains. *Adv. Funct. Mater.* **23**, 198–203 (2013).
9. S. Chen, H. Ji, H. Chou, Q. Li, H. Li, J. W. Suk, R. Piner, L. Liao, W. Cai, R. S. Ruoff, Millimeter-size single-crystal graphene by suppressing evaporative loss of Cu during low pressure chemical vapor deposition. *Adv. Mater.* **25**, 2062–2065 (2013).
10. Y. H. Zhang, Z. Y. Chen, B. Wang, Y. W. Wu, Z. Jin, X. Y. Liu, G. H. Yu, Controllable growth of millimeter-size graphene domains on Cu foil. *Mater. Lett.* **96**, 149–151 (2013).
11. Y. Hao, M. S. Bharathi, L. Wang, Y. Liu, H. Chen, S. Nie, X. Wang, H. Chou, C. Tan, B. Fallahazad, H. Ramanarayan, C. W. Magnuson, E. Tutuc, B. I. Yakobson, K. F. McCarty, Y.-W. Zhang, P. Kim, J. Hone, L. Colombo, R. S. Ruoff, The role of surface oxygen in the growth of large single-crystal graphene on copper. *Science* **342**, 720–723 (2013).
12. T. Wu, X. Zhang, Q. Yuan, J. Xue, G. Lu, Z. Liu, H. Wang, H. Wang, F. Ding, Q. Yu, X. Xie, M. Jiang, Fast growth of inch-sized single-crystalline graphene from a controlled single nucleus on Cu–Ni alloys. *Nat. Mater.* **15**, 43–47 (2016).
13. G. A. Kimmel, J. Matthiesen, M. Baer, C. J. Mundy, N. G. Petrik, R. S. Smith, Z. Dohnálek, B. D. Kay, No confinement needed: Observation of a metastable hydrophobic wetting two-layer ice on graphene. *J. Am. Chem. Soc.* **131**, 12838–12844 (2009).
14. A. Politano, G. Chiarello, Ice formation on clean and alkali-doped quasi-freestanding graphene: A vibrational investigation. *Carbon* **93**, 242–249 (2015).
15. T. O. Wehling, A. I. Lichtenstein, M. I. Katsnelson, First-principles studies of water adsorption on graphene: The role of the substrate. *Appl. Phys. Lett.* **93**, 202110 (2008).
16. X. Li, J. Feng, E. Wang, S. Meng, J. Klimeš, A. Michaelides, Influence of water on the electronic structure of metal-supported graphene: Insights from van der Waals density functional theory. *Phys. Rev. B* **85**, 085425 (2012).
17. X. Feng, S. Maier, M. Salmeron, Water splits epitaxial graphene and intercalates. *J. Am. Chem. Soc.* **134**, 5662–5668 (2012).
18. M. Gulde, S. Schweda, G. Storeck, M. Maiti, H. K. Yu, A. M. Wodtke, S. Schäfer, C. Ropers, Ultrafast low-energy electron diffraction in transmission resolves polymer/graphene superstructure dynamics. *Science* **345**, 200–204 (2014).
19. G. A. Morton, E. G. Ramberg, Point projector electron microscope. *Phys. Rev.* **56**, 705 (1939).
20. J. Y. Mutus, L. Livadaru, J. T. Robinson, R. Urban, M. H. Salomons, M. Cloutier, R. A. Wolkow, Low-energy electron point projection microscopy of suspended graphene, the ultimate 'microscope slide'. *New J. Phys.* **13**, 063011 (2011).
21. X. Lin, P. Liu, Y. Wei, Q. Li, J. Wang, Y. Wu, C. Feng, L. Zhang, S. Fan, K. Jiang, Development of an ultra-thin film comprised of a graphene membrane and carbon nanotube vein support. *Nat. Commun.* **4**, 2920 (2013).
22. L. Lin, L. Sun, J. Zhang, J. Sun, A. L. Koh, H. Peng, Z. Liu, Rapid growth of large single-crystalline graphene via second passivation and multistage carbon supply. *Adv. Mater.* **28**, 4671–4677 (2016).
23. H. Wang, G. Wang, P. Bao, S. Yang, W. Zhu, X. Xie, W.-J. Zhang, Controllable synthesis of submillimeter single-crystal monolayer graphene domains on copper foils by suppressing nucleation. *J. Am. Chem. Soc.* **134**, 3627–3630 (2012).
24. J. M. Cowley, Adjustment of a STEM instrument by use of shadow images. *Ultramicroscopy* **4**, 413–418 (1979).

25. J. M. Cowley, Coherent interference in convergent-beam electron-diffraction and shadow imaging. *Ultramicroscopy* **4**, 435–449 (1979).
26. S.-Y. Wang, J. M. Cowley, Shadow images for in-line holography in a stem instrument. *Microsc. Res. Tech.* **30**, 181–192 (1995).
27. P. Hirsch, A. Howie, R. Nicholson, D. W. Pashley, M. J. Whelan, in *Electron Microscopy of Thin Crystals* (Krieger, New York, ed. 2, 1977), pp. 295–310.
28. J. M. Wofford, S. Nie, K. F. McCarty, N. C. Bartelt, O. D. Dubon, Graphene islands on Cu foils: The interplay between shape, orientation, and defects. *Nano Lett.* **10**, 4890–4896 (2010).
29. Y. Ogawa, B. Hu, C. M. Orofeo, M. Tsuji, K.-i. Ikeda, S. Mizuno, H. Hibino, H. Ago, Domain structure and boundary in single-layer graphene grown on Cu(111) and Cu(100) films. *J. Phys. Chem. Lett.* **3**, 219–226 (2012.
30. R. L. Park, H. E. Farnsworth, CO adsorption and interaction with oxygen on (110) nickel. *J. Chem. Phys.* **40**, 2354–2357 (1964).
31. R. N. Lee, H. E. Farnsworth, LEED studies of adsorption on clean (100) copper surfaces. *Surf. Sci.* **3**, 461–479 (1965).
32. A. J. Pignocco, G. E. Pellissier, Leed studies of oxygen adsorption and oxide formation on an (011) iron surface. *Surf. Sci.* **7**, 261–278 (1967).
33. B. J. Hopkins, M. Leggett, G. D. Watts, A rheed study of the adsorption of oxygen, hydrogen, nitrogen and water vapour on the (100) face of tantalum. *Surf. Sci.* **28**, 581–597 (1971).
34. J. S. Arellano, L. M. Molina, A. Rubio, J. A. Alonso, Density functional study of adsorption of molecular hydrogen on graphene layers. *J. Chem. Phys.* **112**, 8114–8119 (2000).
35. J. Moser, A. Verdaguer, D. Jiménez, A. Barreiro, A. Bachtold, The environment of graphene probed by electrostatic force microscopy. *Appl. Phys. Lett.* **92**, 123507 (2008).
36. O. Leenaerts, B. Partoens, F. M. Peeters, Water on graphene: Hydrophobicity and dipole moment using density functional theory. *Phys. Rev. B* **79**, 235440 (2009).
37. A. Politano, A. R. Marino, V. Formoso, G. Chiarello, Hydrogen bonding at the water/quasi-freestanding graphene interface. *Carbon* **49**, 5180–5184 (2011).
38. A. Politano, A. R. Marino, V. Formoso, G. Chiarello, Water adsorption on graphene/Pt(111) at room temperature: A vibrational investigation. *AIP Adv.* **1**, 042130 (2011).
39. D. J. Anick, Static density functional study of graphene–hexagonal bilayer ice interaction. *J. Phys. Chem. A* **118**, 7498–7506 (2014).
40. S. Standop, T. Michely, C. Busse, H_2O on graphene/Ir(111): A periodic array of frozen droplets. *J. Phys. Chem. C* **119**, 1418–1423 (2015).
41. J. Carrasco, A. Michaelides, M. Forster, S. Haq, R. Raval, A. Hodgson, A one-dimensional ice structure built from pentagons. *Nat. Mater.* **8**, 427–431 (2009).
42. J. Carrasco, A. Hodgson, A. Michaelides, A molecular perspective of water at metal interfaces. *Nat. Mater.* **11**, 667–674 (2012).
43. J. C. Meyer, A. K. Geim, M. I. Katsnelson, K. S. Novoselov, D. Obergfell, S. Roth, C. Girit, A. Zettl, On the roughness of single- and bi-layer graphene membranes. *Solid State Commun.* **143**, 101–109 (2007).
44. P. Hohenberg, W. Kohn, Inhomogeneous electron gas. *Phys. Rev.* **136**, B864–B871 (1964).
45. W. Kohn, L. J. Sham, Self-consistent equations including exchange and correlation effects. *Phys. Rev.* **140**, A1133–A1138 (1965).
46. G. Kresse, J. Furthmüller, Efficient iterative schemes for ab initio total-energy calculations using a plane-wave basis set. *Phys. Rev. B* **54**, 11169–11186 (1996).
47. G. Kresse, D. Joubert, From ultrasoft pseudopotentials to the projector augmented-wave method. *Phys. Rev. B* **59**, 1758–1775 (1999).
48. P. E. Blöchl, Projector augmented-wave method. *Phys. Rev. B* **50**, 17953–17979 (1994).
49. J. P. Perdew, K. Burke, M. Ernzerhof, Generalized gradient approximation made simple. *Phys. Rev. Lett.* **77**, 3865–3868 (1996).
50. J. Klimeš, D. R. Bowler, A. Michaelides, Van der Waals density functionals applied to solids. *Phys. Rev. B* **83**, 195131 (2011).
51. K. Lee, É. D. Murray, L. Kong, B. I. Lundqvist, D. C. Langreth, Higher-accuracy van der Waals density functional. *Phys. Rev. B* **82**, 081101 (2010).
52. H. J. Monkhorst, J. D. Pack, Special points for Brillouin-zone integrations. *Phys. Rev. B* **13**, 5188–5192 (1976).

Acknowledgments: We thank X. H. Yang, X. H. Wang, J. Zhang, Y. Wu, B. C. Du, Y. Wei, K. Liu, and J. P. Wang for valuable discussions. We thank D. L. Zhou for help in the LEED experiments and the construction of the diffraction instrument. We thank Y. J. Yan for help in the electron backscatter diffraction (EBSD) characterization of the copper foil. We thank L. Y. Zhao, X. Fan, and H. W. Wang for help in the cryo-TEM characterization of adsorbates on graphene. **Funding:** This work was supported by the National Basic Research Program of China (no. 2012CB932301), the National Natural Science Foundation of China (nos. 11321091, 51672152, 51472142, 11274190, and 21433006), the National Thousand-Young-Talents Program, and Tsinghua University Initiative Scientific Research Program. **Author contributions:** P. Liu and K.J. conceived the experiments. P. Liu and W.Z. performed the LEED experiments. X.L. and W.Z. performed the polycrystalline graphene synthesis and graphene transfer. L.L., H.P., and Z.L. performed the single-crystal graphene synthesis. W.Z. performed the single-crystal graphene transfer. X.X. and Q.L. performed the MoS_2 synthesis. W.Z. and P. Lei performed the MoS_2 transfer. L.Z., W.Z., and P. Liu performed the TEM characterization. W.Z. and P. Liu performed the EBSD characterization. B.X., Y.X., W.D., and M.Z. performed the calculations of adsorption structures. Y.Z. and R.Y. performed the simulation of diffraction patterns. P. Liu fabricated the compact instrument for low-energy transmission electron diffraction and imaging. P. Liu, K.J., and W.Z. analyzed the experiment results and data. L.P. and J.W. gave advice on diffraction experiments. P. Liu, K.J., W.Z., Y.X., and B.X. wrote the manuscript. K.J. and S.F. supervised the project. All authors discussed the results and commented on the manuscript. **Competing interests:** P. Liu, W.Z., X.L., K.J., and S.F. are authors on a patent application related to this work filed by Tsinghua University and Hongfujin Precision Industry Corporation (Shenzhen) Ltd. (application no. 201610404782.4, filed 8 June 2016). The other authors declare that they have no competing interests. **Data and materials availability:** All data needed to evaluate the conclusions in the paper are present in the paper and/or the Supplementary Materials. Additional data related to this paper may be requested from the authors.

Submitted 20 December 2016
Accepted 7 August 2017
Published 1 September 2017
10.1126/sciadv.1603231

Citation: W. Zhao, B. Xia, L. Lin, X. Xiao, P. Liu, X. Lin, H. Peng, Y. Zhu, R. Yu, P. Lei, J. Wang, L. Zhang, Y. Xu, M. Zhao, L. Peng, Q. Li, W. Duan, Z. Liu, S. Fan, K. Jiang, Low-energy transmission electron diffraction and imaging of large-area graphene. *Sci. Adv.* **3**, e1603231 (2017).

Science Advances

Low-energy transmission electron diffraction and imaging of large-area graphene

Wei Zhao, Bingyu Xia, Li Lin, Xiaoyang Xiao, Peng Liu, Xiaoyang Lin, Hailin Peng, Yuanmin Zhu, Rong Yu, Peng Lei, Jiangtao Wang, Lina Zhang, Yong Xu, Mingwen Zhao, Lianmao Peng, Qunqing Li, Wenhui Duan, Zhongfan Liu, Shoushan Fan and Kaili Jiang

Sci Adv **3** (9), e1603231.
DOI: 10.1126/sciadv.1603231